Phytoplankton distribution related to different winter conditions in 2016 and 2017 in the open southern Adriatic Sea (eastern Mediterranean)

Nenad Jasprica [a],[*],[1], Marijeta Čalić [a],[1], Vedrana Kovačević [b], Manuel Bensi [b], Iris Dupčić Radić [a], Rade Garić [a], Mirna Batistić [a]

[a] University of Dubrovnik, Institute for Marine and Coastal Research, Dubrovnik, Croatia
[b] National Institute of Oceanography and Applied Geophysics - OGS, Sgonico, Trieste, Italy

A B S T R A C T

Phytoplankton community structure and dynamics were investigated in the open southern Adriatic Sea during two winter-spring seasons (2016 and 2017) under different oceanographic and meteorological conditions. The principal environmental factor was a pronounced inflow of the Levantine Intermediate Water into the Adriatic, favoured by the cyclonic circulation of the Northern Ionian Gyre. As a consequence, high salinity values of about 38.8–38.9, were registered. Fifteen research cruises were undertaken in the same sampling area situated in the northern part of the Southern Adriatic Pit (SAP) with a maximum depth of 1200 m. Two specific circumstances were encountered: (i) high abundances of phytoplankton in the deep layer associated with strong downward flow in 2016, and (ii) an intense surface phytoplankton bloom in March 2017. This particular event occurred following the strong vertical convective mixing, which increased nutrient availability in the euphotic layer. High in situ Chl-*a* concentrations (max. 1.65 mg m^{-3}) and phytoplankton abundances higher than 10^5 cells L^{-1} are not common in the habitually oligotrophic open southern Adriatic Sea, and this study attempts to determine the driving force of that phenomenon. The phytoplankton community in SAP involved nanoflagellates and diatoms as the most abundant taxonomic groups during the March 2017 bloom. Presence of some coastal phytoplankton taxa suggests the influx of coastal water masses and transport of species either longitudinally, from the northern to the Southern Adriatic in concomitance of the Northern Adriatic Dense Water spreading, or transversal as a response to the strong mesoscale activity in the study region, comprising intense shelf - open sea interaction.

1. Introduction

The Adriatic Sea, the northernmost part of the Mediterranean, is a semi-enclosed basin whose ecosystems are largely influenced by regular water exchange with the Ionian Sea through the Strait of Otranto (~80–100 km wide, and a sill of about 800 m deep). The key area of that exchange is the southern Adriatic basin with its deepest part (the South Adriatic Pit, hereafter SAP), ~1250 m deep, where not only dense waters form during harsh winters, but also dense waters originating from the northern Adriatic accumulate. The southern Adriatic basin is characterized by the presence of a quasi-permanent cyclonic circulation (Gačić et al., 2002).

Levantine Intermediate Water (LIW) and Ionian Surface Water (ISW) flow into the SAP along the eastern side of the southern Adriatic basin (Poulain and Cushman-Roisin, 2001). On its western side, instead, a mix

of the Adriatic Dense Water (AdDW) and Northern Adriatic Dense Water (NAdDW) flows out through the Strait of Otranto and sinks into the abyssal Ionian Sea, playing an important role as primary source of the Eastern Mediterranean Deep Water (EMDW, Robinson et al., 2001; Rubino and Hainbucher, 2007; Bensi et al., 2013). The formation of water masses in the Adriatic Sea, as well as the volume and properties of the dense water outflow passing through the Strait of Otranto vary on an interannual time scale as a function of long-term thermohaline changes, local meteorological conditions, and climatic oscillations in the whole eastern Mediterranean (Grbec et al., 2002; Vilibić and Orlić, 2002; Manca et al., 2003; Ursella et al., 2011; Yari et al., 2012). Long-term research has shown that the interaction between the Adriatic and Ionian Seas resembles the Bimodal Oscillating System (BiOS) that changes the circulation of the Northern Ionian Gyre (NIG) from the cyclonic to the anticyclonic mode and vice versa, affecting thermohaline

and biogeochemical properties in the southern Adriatic at decadal scale (Civitarese et al., 2010; Gačić et al., 2010; Gačić and Civitarese, 2012). When the NIG is anticyclonic, Atlantic Water (AW) with lower salinity/density enters the SA along with nutrient-rich waters in the layer of 200–800 m depth. When the NIG is cyclonic, the northern branch of the AW flow attenuates or ceases, and the advection of saltier/denser but nutrient-poor LIW into the southern Adriatic prevails (Vilibić and Orlić, 2002; Civitarese et al., 2010). These physical concepts have an important consequence on shifts in primary production and biodiversity in the SAP area (Civitarese et al., 2010; Batistić et al., 2014; Ljubimir et al., 2017).

The offshore ecosystem of the southern Adriatic is truly pelagic with low impact of coastal waters on the amount of nutrients (Viličić et al., 1995; Gačić et al., 1999). According to Gačić et al. (2002) and Civitarese et al. (2010), primary production in this area appears to be mostly controlled by changes in meteorological conditions that determine convective mixing and the amount of nutrients available for autotrophic consumption. Vertical convection occurs in winter or early spring because of the buoyancy loss by cooling and evaporation at the air-sea interface, increasing the density of the surface waters (Boldrin et al., 2002). So far, in general, the SAP has been considered as clearly oligotrophic with low phytoplankton abundance and biomass (Viličić, 1998).

Until the mid-2000s, data on the phytoplankton community in the open southern Adriatic (OSA) were mainly based on episodic samplings, with long gaps in some periods (e.g., 1998–2006). Some investigations carried out in the last decade contributed to advancing knowledge on the phytoplankton dynamic and structure, particularly in winter-spring seasons (see Ljubimir et al., 2017; Batistić et al., 2019).

Phytoplankton maxima appearing mostly in spring (Viličić et al., 1989; Viličić, 1998; Socal et al., 1999; Turchetto et al., 2000; Santoleri et al., 2003; Cerino et al., 2012). Batistić et al. (2012) proved that OSA is not exclusively oligotrophic, but subject to ordinary winter phytoplankton blooms, whose intensity depends as previously mentioned, on specific hydroclimatic events. Due to that particular occasions linked to wind–induced mixing and vertical convection, and consequent nutrient input into the euphotic zone of SAP, high interannual variability in phytoplankton abundance may occur (Viličić et al., 1989; Santoleri et al., 2003; Ljubimir et al., 2017). More recently, Batistić et al. (2019) concluded that winter blooms are persistent features of the OSA and they can occur during both anticyclonic and cyclonic phases of the NIG, but driven by different mechanisms.

However, according to the oligotrophic character during most of the year, nanophytoplankton and picophytoplankton are the most abundant primary producers in the SAP (Batistić et al., 2012; Cerino et al., 2012; Najdek et al., 2014; Babić et al., 2017; Šilović et al., 2018). In OSA, except during the periods of vertical mixing, microphytoplankton is the most abundant in the layer of the subsurface Chl-*a* maximum (Jasprica et al., 2001; Batistić et al., 2012; Cerino et al., 2012; Ljubimir et al., 2017).

The main objective of this study is to analyze the time evolution of the dynamic and the community structure of phytoplankton assemblages in OSA during winter-spring seasons, in two years (2016 and 2017) characterized by different hydroclimatic situations. A second objective is to couple them with bloom formation in highly dynamic winter-spring periods. Specific tasks were: (i) to describe the spatio-temporal pattern of nutrients and phytoplankton in relation to the hydrographic properties of the water column; (ii) to characterize the main environmental factors which control the distribution of phytoplankton abundance and species composition; (iii) to describe the mechanisms of phytoplankton late winter-bloom formation.

2. Materials and methods

2.1. Field data collection

The field study was conducted in two winter-spring periods, i.e.,

from January to May at station P-1200 (42°13′01.0″ N, 17°42′50.0″ E) in the SAP (Fig. 1). In 2016, samples were collected on 16th and 28th January, 24th February, 20th March, 21st April and 27th May. In 2017, sampling was conducted on 20th January, 8th and 17th February, 3rd, 20th and 24th March, 5th April, 4th and 24th May. Altogether, 15 research cruises were undertaken and 202 samples of nutrients, and 147 in each chlorophyll-*a* concentrations (Chl-*a*) and phytoplankton were respectively analysed.

Temperature (°C) and salinity vertical profiles were taken with a conductivity-temperature-depth (CTD) multi-parametric probe (Sea-Bird Electronics Inc., USA) from the surface to approximately 1200 m depth. Data were averaged every 1 m during post processing. The fluorescence sensor (WETLABS fluorometer) was used to estimate the Chl-a content (mg m^{-3}) in the water column. Water samples were taken with 5-L Niskin bottles for dissolved oxygen, nutrients, Chl-*a* and phytoplankton analyses. Nutrient samples were collected without filtering. Nutrients, phytoplankton and Chl-*a* were sampled at 0, 5, 10, 20, 50, 75, 100, 150 and 200 m in each cruise and additionally at 300, 400, 600, 800 m when Chl-*a* signal detected with fluorescence sensor was deeper than 200 m. Samples for dissolved oxygen and nutrient analysis were taken even at 1000 and 1200 m.

2.2. Analysis methods

Derived parameters such as potential temperature (θ) and potential density anomaly (σ_θ, kg m^{-3}) referred to 0 dbar were calculated from original data using TEOS-10 Gibbs function approach within the Ocean Data View application (Schlitzer, 2020).

Dissolved oxygen was determined by Winkler titration and oxygen saturation rate (O_2/O_2') was calculated from solubility of oxygen in seawater as a function of the corresponding temperature and salinity (Weiss, 1970; UNESCO, 1987). Chemical parameters included phosphate (PO_4), nitrate (NO_3), nitrite (NO_2), ammonium (NH_4) and silicate (SiO_4). Samples for NO_3, NO_2, PO_4 and SiO_4 were frozen (-22 °C) immediately after sampling. Samples remained frozen until the night before analysis, when they were defrosted at room temperature and analysed according to Strickland and Parsons (1972) using spectro-photometer PerkinElmer Lambda 15 (Ueberlingen, Germany).
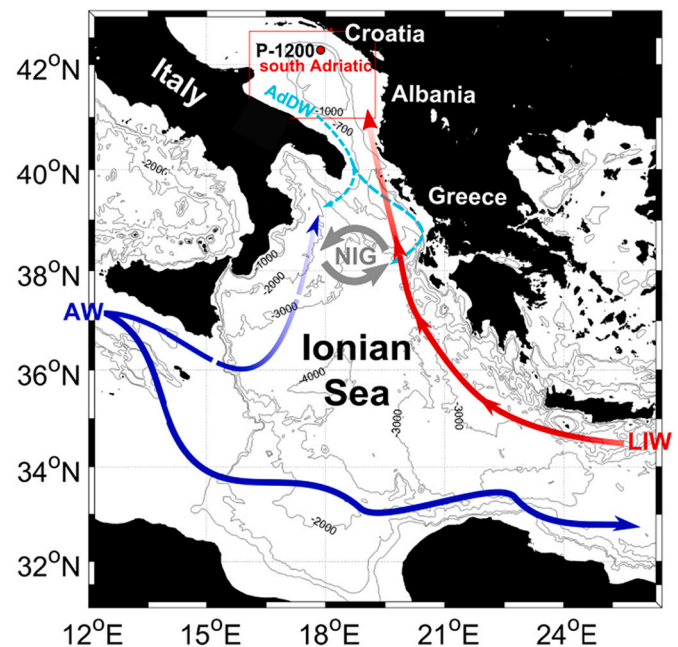

Fig. 1. Location of P-1200 sampling station in the open southern Adriatic Sea. The circulation regime in the Ionian Sea is also shown. NIG – North Ionian Gyre, AW – Atlantic Water, LIW – Levantine Intermediate Water.

Subsamples for NH_4 (50 mL) were fixed immediately after collection on board with 1 mol L^{-1} phenol/EtOH, kept at 4 °C and analysed according to Ivančić and Degobbis (1984). Total inorganic nitrogen (TIN) was calculated as the sum of NO_3, NO_2 and NH_4.

To estimate Chl-*a* concentrations (mg m^{-3}) 1 L water sub-samples were filtered through Whatman GF/F glass-fiber filters and stored at −20 °C. Then, they were homogenized and extracted in 90% acetone for 24 h at room temperature (Holm-Hansen et al., 1965). Finally, samples were analysed fluorometrically with a Turner TD-700 Laboratory Fluorometer (Sunnyvale, CA) calibrated with pure Chl-*a* (Sigma).

To estimate surface chlorophyll concentration over the southern Adriatic Sea during winters 2016 and 2017, data from the Moderate Resolution Imaging Spectroradiometer (Aqua MODIS, L3SMI, Global, 4 km resolution, NASA's Aqua Spacecraft) were used. These data are freely available from the NOAA ERDDAP platform.

Phytoplankton samples ($N = 50$ in 2016 and $N = 101$ in 2017) were preserved in neutralized formaldehyde (2.5% final concentration) and observed with an Olympus IX-71 inverted microscope according to the Utermöhl method (Utermöhl, 1958). Subsamples (100 mL) were settled for 48 h in counting chambers (Hydro-Bios) before analysis. Phytoplankton cells, excluding nanoflagellates, were counted at a magnification of 200× in three central transects and at 100× over the entire area of the counting chamber base plate. Nanoflagellates were counted in at least 30 randomly selected fields along the chamber bottom at 600× by using phase contrast. The phytoplankton abundances are expressed as a number of cells per liter (cells L^{-1}). Whenever possible, phytoplankton was identified to the species or genus level using standard keys, monographs and taxonomic guides (for details see Ljubimir et al., 2017). The nomenclature of taxa follows AlgaeBase (Guiry and Guiry, 2020). Phytoplankton (cells longer than 2 μm) was divided into six groups: diatoms (Bacillariophyta), coccolithophorids (Coccolithophyceae), dinoflagellates (Dinophyceae), silicoflagellates (Dictyochophyceae), nanoflagellates (NFL), and chlorophytes (Pyramimonadophyceae, Chlorophyta). The latter group was composed solely of species *Halosphaera viridis* F.Schmitz. NFL cells were not taxonomically identified at genus/species level. The rare taxon *Leucocryptos marina* (Braarud) Butcher (Katablepharidophyta) was excluded from the analyses due to its exceptional rarity.

Meteorological data (i.e., air temperature, °C; wind speed in m s^{-1} and direction, °N) recorded at the nearest coastal station in Dubrovnik between January 2016 and December 2017 were provided by the Croatian Meteorological and Hydrological Service. Such data can be considered representative also for the open sea area near station P-1200, which is about 50 km distant from the coast. As a verification, we compared the station data with the ECMWF-ERA 5 wind field in the OSA gathered from the European Centre for Medium-Range Weather Forecasts datasets (doi: 10.24381/cds.adbb2d47), obtaining a good agreement in terms of temporal variability (not shown). Here we refer to data collected between January and May 2016 (JFMAM) and between January and May 2017 (JFMAM) that cover the two periods during which oceanographic data were collected.

2.3. Data analysis

Cluster analysis was used to analyze the variability in abundances of the phytoplankton taxa (Legendre and Legendre, 1983). Cluster analysis was based on the matrix consisting of 222 taxa × 151 samples over 15 sampling dates. The analysis excluded nanoflagellates. An agglomerative, hierarchical clustering algorithm based on Bray-Curtis similarity matrix and Ward's method for determination of group linkages was used. Abundances of phytoplankton taxa were standardized and logarithmically transformed [log (x + 1)] before analysis. Statistical analyses were performed using PRIMER v6 software (Clarke and Gorley, 2006).

Canonical Correspondence Analysis (CCA) was used to relate the abundance of phytoplankton taxa to 11 environmental variables (ter Braak and Verdonschot, 1995). In 2016, a dataset of 34 phytoplankton

taxa found in more than 11% of the total number of samples ($n = 47$) was selected for this analysis. In 2017, 37 taxa have been taken into consideration (found in more than 15% in total number of samples, $n = 91$). Neither transformation (e.g., square root or log) of species data nor down-weighting of rare species was performed. The data were centered and standardized before analyses as they were measured on different scales. A Monte Carlo permutation test (reduced model–499 permutations) was used to test the statistical significance of each variable (expressed with F and *P* value). The analysis was carried out using CANOCO for Windows 4.52 software (ter Braak and Šmilauer, 2002).

3. Results

3.1. Meteorological conditions during winters 2016 and 2017

The prevailing winds in this study area come from the 1st quadrant (0°-90°, prevalently NE bora wind) and 2nd quadrant (90°-180°, prevalently SE sirocco winds). The winter of 2016 was characterized by a higher frequency of easterly and SE winds, with respect to winter 2017 (Fig. 2a), which in turn had more frequent and long-lasting NE wind events.

During both winters, the coldest weather conditions occurred in January, when air temperature decreased below 0 °C. These events were associated with strong, cold and dry Bura (NE) wind, which in January 2017 was more intense (wind speed >20 m s^{-1}, with gusts >35 m s^{-1}) than in 2016 (wind gusts up to ~33 m s^{-1}). The strongest NE wind episode occurred in the first half of January 2017 and lasted about 11 days, during which for 6–7 days air temperatures were below 0 °C.

In mid February 2016 air temperature increased to more than 20 °C for about one week characterized by the persistence of moderate SE winds (10 m s^{-1} with peaks up to 18–20 m s^{-1}). Air temperatures above 20 °C were also recorded at the end of March 2017, exceptionally in this case associated with short lasting but moderate NE winds.

3.2. Hydrography

The two years showed peculiar thermohaline characteristics, which distinguish them from each other (Fig. 3).

As far as temperature is concerned, January periods were pretty uniform in the upper 200 m. However, in 2016 the temperature was higher (14.4–14.5 °C) than in 2017 (14.2 °C). The deepening of the isotherm of 14 °C indicates that during the winter time (Jan-Mar) vertical convection and mixing reached depths of about 700–800 m in 2017, and not more than 500 m in 2016.

Throughout winter-spring 2016 the salinity distribution in the upper 200 m had values ranging between 38.76 and 38.84. The layer between 200 and 400 m depth, instead, had lower salinity values (minimum 38.74) during January and February, while in March meteorological events caused vertical mixing down to 400 m depth, and consequent homogenous salinity distribution. Between 400 and 700 m depth, salinity values were higher, about 38.84, while from there down to the bottom, salinity gradually diminished to a minimum of about 38.72.

In December 2016 salinity distribution was not uniform, with layers of alternating high and low values (not shown). This vertical structure was destroyed in January 2017 after the first harsh meteorological event of the season (see Fig. 2), which contributed to mixing the upper 700 m layer, leading to temperatures of about 14 °C and salinity of about 38.80–38.82. As a consequence of this strong convective event, the double salinity maximum observed in 2016, disappeared and the relative maximum in salinity remained confined only in the upper 100–150 m layer during the following months. The deep layer, below 800 m depth, was characterized by lower temperature and salinity (and density) values in 2017 than in 2016. However, in May 2017, in the bottom layer, temperature and salinity suddenly increased from 13.12–13.14 °C to about 13.26 °C and from 38.72 to 38.76–38.77. Density also increased from 29.25 kg m^{-3} to 26.26 kg m^{-3} (not shown).
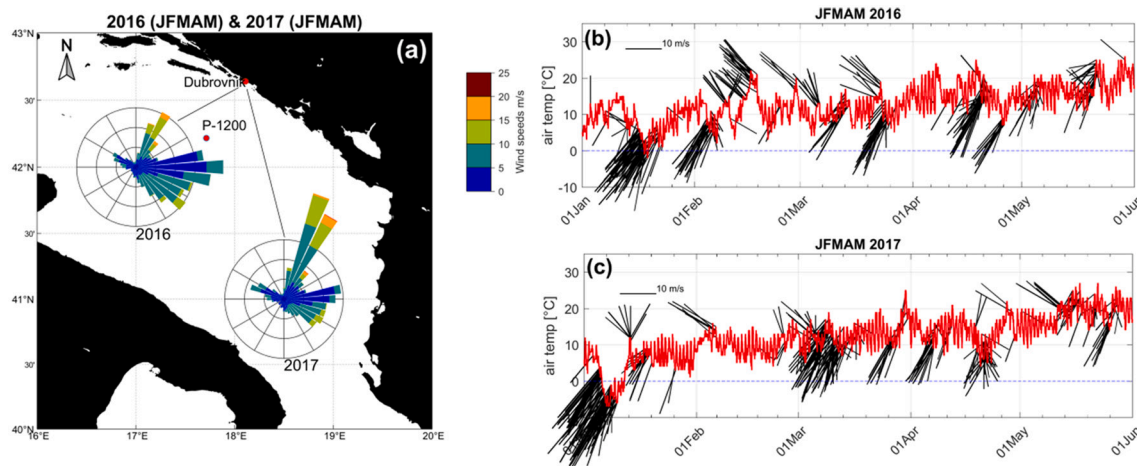
Fig. 2. (a) Map of the southern Adriatic with the location of the meteorological land-station and marine station P-1200 (red dots), and the wind rose diagrams (wind provenance) referred to 2016 (JFMAM) and 2017 (JFMAM); (b, c) Time series of air temperature (°C, red line) and wind (m s^{-1}) during strong events (when gusts are >10 m s^{-1}). Black lines indicate the direction the wind is going to (with respect to North). (For interpretation of the references to color in this figure legend, the reader is referred to the web version of this article).

The temporal variability of dissolved oxygen distribution deserves special attention, since it is strongly influenced by vertical convection events and, in turn, influences the development and distribution of phytoplankton species. During February-May 2016, the upper/intermediate layer (0–500 m depth) of the water column at station P-1200 was characterized by high oxygen content (saturation rate > 1). In March 2016, the ventilation reached 400–500 m, while in January and February 2017 it reached about 700–800 m depth, even though in general maximum values were lower than those recorded in 2016 in the upper layer (0–200 m). As far as the deep layer (> 800 m depth) is concerned, there were no significant oxygen variations, but a slight increase of the oxygen saturation rate was recorded in early spring in both years.

3.3. Nutrients

Total inorganic nitrogen (TIN) concentrations ranged from 0.41 to 3.56 μM (average, avg. 1.51 μM) in 2016 and from 0.23 to 3.53 μM in 2017 (avg. 1.55 μM) (Fig. 4). In general, NO$_3$ accounted for the highest proportion of TIN during both winter-spring periods with an average of 72.9% in 2016 and 74.6% in 2017, respectively. Relative contribution of NH$_4$ reached maximum only in a few spring samples during both years at some depths up to 200 m (avg. 23.6% in 2016 and 21.6% in 2017). NO$_2$ generally was almost negligible with an average of 3.5% in 2016 and 3.4% in 2017, respectively.

In 2016, phosphate (PO$_4$) was mostly in range 0.04–0.36 μM (avg. 0.15 μM) except higher value recorded in May at 10 m (0.53 μM). In 2017, PO$_4$ mostly ranged from 0.03 to 0.42 μM (avg. 0.20 μM). The highest values (0.54–1.13) were observed in February (17th) and March (24th) at some depths ≥50 m.

Silicate (SiO$_4$) ranged from 1.57 μM in May at 10 m to 10.71 μM in January in the bottom layer (avg. 4.05 μM) in 2016. In 2017, SiO$_4$ ranged from 0.92 in the end of May to 13.28 μM in the second half of March (avg. 3.78 μM). In addition to the greatest depths, high SiO$_4$ concentrations (9.49–13.28 μM) were also recorded in March 2017 at some depths in the upper 100 m when PO$_4$ concentrations were also increased.

3.4. Phytoplankton community structure and abundance

Altogether, 228 phytoplankton taxa were identified in the samples, of which 34 and 62 were only found in 2016 and 2017, respectively (Table 1). There were 132 taxa common to both winter-spring periods.

In total, 109 and 92 taxa belong to the dinoflagellates and diatoms, respectively. These include 48 genera of diatoms and 34 genera of dinoflagellates. Genera with the greatest number of taxa (species and infraspecific taxa) were: *Chaetoceros* (19), *Tripos* and *Protoperidinium* (18 each), *Oxytoxum* and *Gonyaulax* (8 each), *Bacteriastrum*, *Dinophysis* and *Prorocentrum* (6 each), etc. Unidentified pennate diatoms and *Nitzschia* spp. were the most frequent taxa with their contribution to the total number of samples during both winter-spring periods from 87% to 94% and 75% to 88%, respectively (Supplementary material S-1). Other phytoplankton groups included the following number of identified taxa: coccolithophorids, 21; silicoflagellates, 2; and chlorophytes, 1 (Table 1).

In general, phytoplankton abundances expressed as 0–200 m water column mean were lower in 2016 (from 6.1 × 10^4 cells L^{-1} in February to 1.3 × 10^5 cells L^{-1} in April; a mean value of all sample scores was 8.2 × 10^4 cells L^{-1}) than in 2017 (from 4.4 × 10^4 cells L^{-1} in January to 1.6 × 10^5 cells L^{-1} in March; a mean value of all sample scores was 1.3 × 10^5 cells L^{-1}). Phytoplankton abundances varied from 2.2 × 10^4 cells L^{-1} to 6.6 × 10^5 cells L^{-1} in 2016 and from 2.2 × 10^4 cells L^{-1} to 3.6 × 10^5 cells L^{-1} in 2017 (Fig. 5). In 2016, both the highest and the lowest phytoplankton abundances were observed in April at 20 m and 150 m depth, respectively. Further, increased phytoplankton abundances (> 1.0 × 10^5 cells L^{-1}) were found in deeper layer (100–300 m depth) from end of January to March. In 2017, the highest phytoplankton abundances were mostly noted between surface and 20 m depth (20th March), and the lowest was at 400 m (8th February). Cluster analysis indicated two main groups (clusters) of samples: (i) samples collected during diatom bloom event (March 2017), (ii) those collected in winter (January-February) and spring (March-April-May) in both years (Supplementary material S-2).

Phytoplankton communities were mainly composed of nanoflagellates (NFL) and diatoms (Fig. 5, Supplementary material S-3). NFL varied from 2.2 × 10^4 cells L^{-1} to 6.6 × 10^5 cells L^{-1} in 2016 and from 2.2 × 10^4 cells L^{-1} to 2.0 × 10^5 cells L^{-1} in 2017 (Fig. 5). Diatom abundance varied from 1.3 × 10^2 cells L^{-1} to 4.7 × 10^4 cells L^{-1} in 2016 and from 2.2 × 10^4 cells L^{-1} to 2.0 × 10^5 cells L^{-1} in 2017. Coccolithophorids formed the third most abundant group with the maximum values of 4.5 × 10^3 cells L^{-1} in 2016 and 6.9 × 10^3 cells L^{-1} in 2017. Maximum abundances of dinoflagellates (2.8 × 10^3 cells L^{-1}), silicoflagellates (6.6 × 10^3 cells L^{-1}) and chlorophytes (1.8 × 10^2 cells L^{-1}) did not differ between two winter-spring periods.

NFL contributed to phytoplankton abundances from 94 to 98% in 2016 and 58 to 98% in 2017, respectively (Supplementary material S-3). Among NFL, small cells (2–10 μm) prevailed (>88%) during both

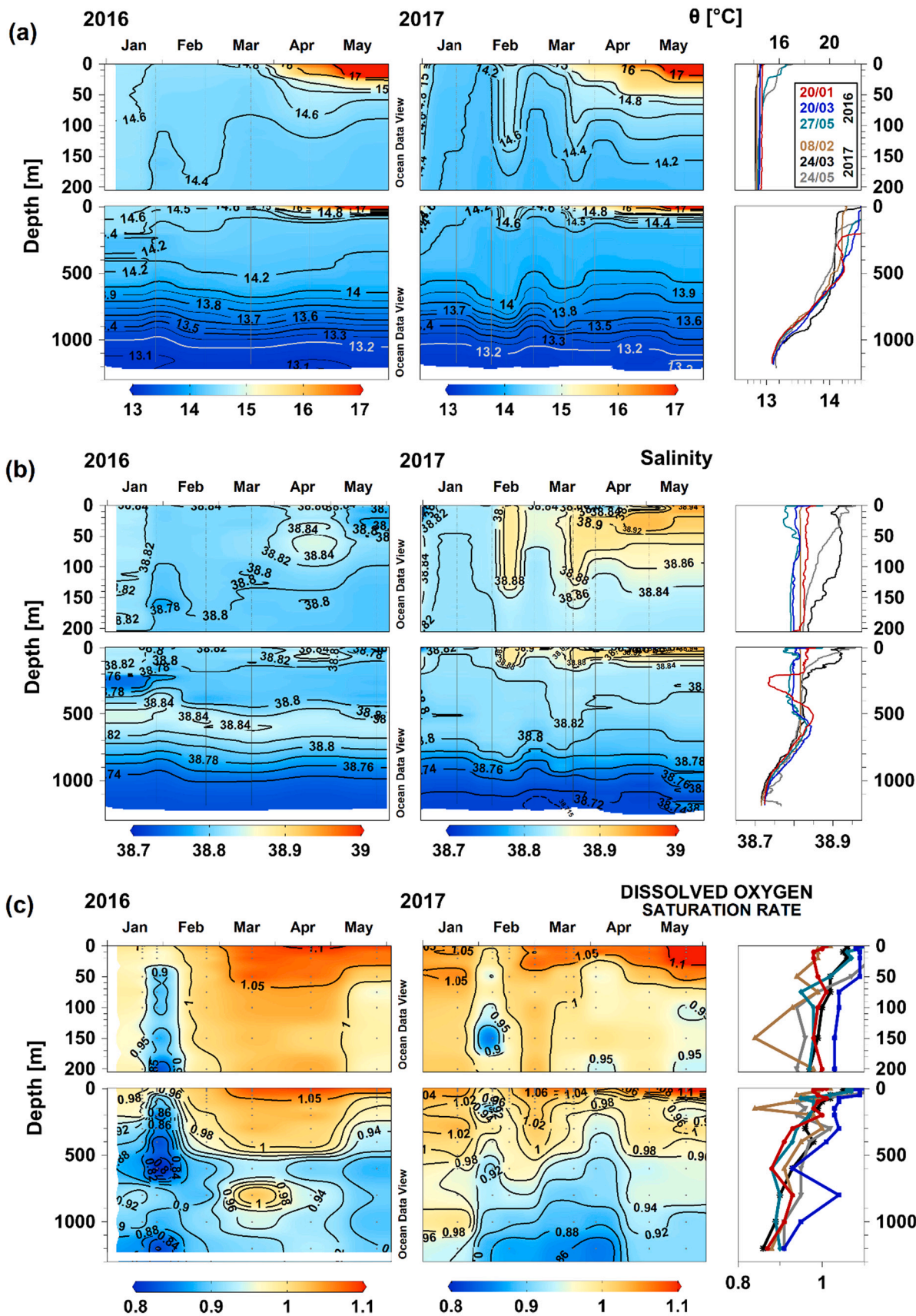**Fig. 3.** Station P-1200 in the open southern Adriatic Sea: time evolution (on the left-hand side) and selected vertical profiles (on the right-hand side) of potential temperature θ (a), salinity S (b), and dissolved oxygen saturation rate O_2/O_2' (c). Time color code for selected profiles is indicated in (a), upper right panel. Topmost panels zoom into the upper 200 m. Vertical resolution (vertical grey lines/dots): θ and S were measured at 1 m intervals, while O_2/O_2' at standard oceanographic depths.
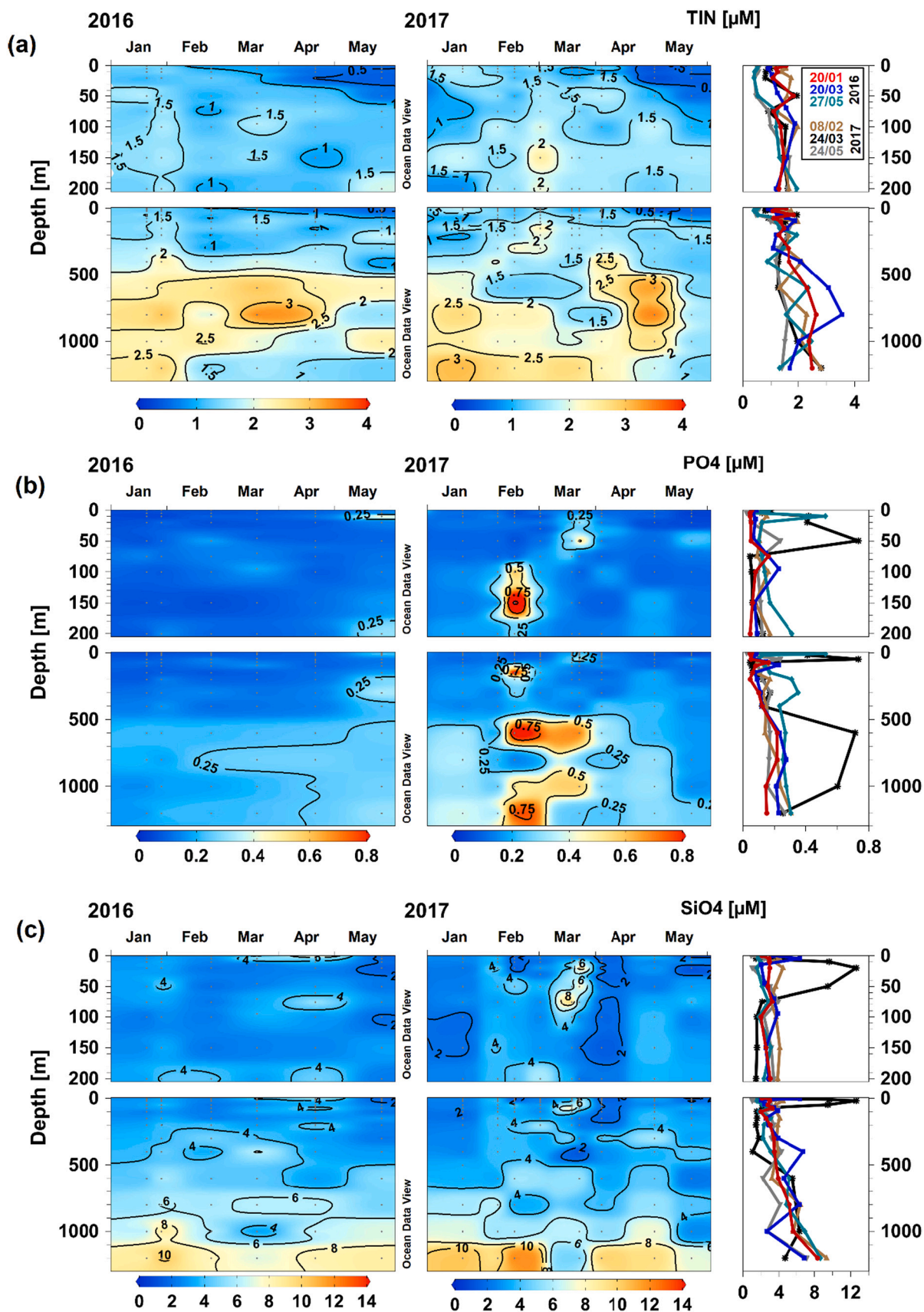
Fig. 4. Station P-1200 in the open southern Adriatic Sea: time evolution (on the left-hand side) and selected vertical profiles (on the right-hand side) of total inorganic nitrogen – TIN (a), phosphate – PO$_4$ (b) and silicate – SiO$_4$ (c) concentrations. Time color code for selected profiles is indicated in (a), upper right panel. Topmost panels zoom into the upper 200 m. Samples were taken at standard oceanographic depths (dots).

Table 1

List of 228 microphytoplankton taxa found at P-1200 sampling station in the open southern Adriatic Sea during the winter-spring period in 2016 and 2017.

Dictyochophyceae

Dictyocha fibula Ehrenberg
Octactis octonaria (Ehrenberg) Hovasse [2017]

Coccolithophyceae

Acanthoica quattrospina Lohmann
Calciopappus caudatus K.R.Gaarder & Ramsfjell [2017]
Calciosolenia brasiliensis (Lohmann) J.R. Young
Calciosolenia murrayi Gran
Calyptrosphaera oblonga Lohmann
Coccolithus pelagicus (Wallich) J.Schiller
Coronosphaera mediterranea (Lohmann) Gaarder
Heimiella excentrica Lohmann
Helicosphaera carteri (Wallich) Kamptner
Michaelsarsia adriatica (Schiller) Manton, Bremer & Oates
Ophiaster hydroideus Lohmann
Pontosphaera syracusana Lohmann
Rhabdolithes claviger (G.Murray & Blackman) Voeltzkow
Rhabdosphaera tignifer Schiller
Rhabdosphaera sp. [2017]
Scyphosphaera apsteinii Lohmann
Syracosphaera histrica Kamptner
Syracosphaera pulchra Lohmann
Syracosphaera sp. [2017]
Umbilicosphaera sibogae (Weber-van Bosse) Gaarder
Other unidentified Coccolithophyceae >20 mm

Pyramimonadophyceae

Halosphaera viridis F.Schmitz

Katablepharidaceae

Leucocryptos marina (Braarud) Butcher [2017]

Bacillariophyta

Coscinodiscophyceae
 Actinocyclus octonarius var. *tenellus* (Brébisson) Hendey [2016]
 Asterolampra marylandica Ehrenberg [2016]
 Asterionellopsis glacialis (Castracane) Round
 Asteromphalus heptactis (Brébisson) Ralfs [2017]
 Coscinodiscus perforatus Ehrenberg [2016]
 Coscinodiscus thorii Pavillard [2017]
 Coscinodiscus spp.
 Dactyliosolen blavyanus (H.Peragallo) Hasle [2017]
 Dactyliosolen fragilissimus (Bergon) Hasle [2017]
 Guinardia flaccida (Castracane) Peragallo [2017]
 Guinardia striata (Stolterfoth) Hasle [2017]
 Guinardia delicatula (Cleve) Hasle [2017]
 Melosira nummuloides C.Agardh [2016]
 Neocalyptrella robusta (G.Norman ex Ralfs) Hernández-Becerril & Meave del Castillo [2016]
 Paralia sulcata (Ehrenberg) Cleve
 Proboscia alata (Brightwell) Sundström
 Pseudosolenia calcar-avis (Schultze) B.G.Sundström
 Rhizosolenia imbricata Brightwell
Bacillariophyceae
 Amphora spp. [2017]
 Bacillaria paxillifera (O.F.Müller) T.Marsson
 Campylodiscus sp.
 Cocconeis sp. [2016]
 Cylindrotheca closterium (Ehrenberg) Reimann & J.C.Lewin
 Diploneis bombus (Ehrenberg) Ehrenberg
 Diploneis spp.
 Entomoneis gigantea (Grunow) Nizamuddin [2017]
 Entomoneis spp.
 Fragilaria sp.
 Gyrosigma balticum (Ehrenberg) Rabenhorst [2017]
 Gyrosigma spp.
 Licmophora arcuata Car & Herwig [2017]
 Licmophora spp.
 Lioloma pacificum (E. Cupp) G.R. Hasle
 Lithodesmium undulatum Ehrenberg [2017]
 Navicula distans (W.Smith) Ralfs

Table 1 (*continued*)

Bacillariophyta

Navicula spp.
Nitzschia incerta (Grunow) M.Peragallo
Nitzchia cf. *incurva* [2017]
Nitzschia longissima (Brébisson) Ralfs
Nitzschia spp.
Surirella sp.
Pleurosigma angulatum (J.T.Quekett) W.Smith
Pleurosigma elongatum W.Smith
Pseudo-nitzschia spp.
Synedra fulgens (Greville) W.Smith [2016]
Thalassionema frauenfeldii (Grunow) Tempère & Peragallo
Thalassionema nitzschioides (Grunow) Mereschkowsky
Tryblionella compressa (J.W.Bailey) Poulin [2017]
Mediophyceae
Bacteriastrum biconicum Pavillard[2017]
Bacteriastrum furcatum Shadbolt
Bacteriastrum hyalinum Lauder [2017]
Bacteriastrum delicatulum Cleve
Bacteriastrum mediterraneum Pavillard [2017]
Bacteriastrum sp. [2017]
Biddulphia sp. [2016]
Chaetoceros affinis Lauder
Chaetoceros anastomosans Grunow
Chaetoceros brevis F.Schütt [2017]
Chaetoceros compressus Lauder
Chaetoceros contortus F.Schütt
Chaetoceros convolutus Castracane [2017]
Chaetoceros costatus Pavillard [2017]
Chaetoceros curvisetus Cleve [2017]
Chaetoceros danicus Cleve [2017]
Chaetoceros decipiens Cleve
Chaetoceros dichaeta Ehrenberg [2017]
Chaetoceros didymus Ehrenberg [2017]
Chaetoceros diversus Cleve [2016]
Chaetoceros lauderi Ralfs ex Lauder [2017]
Chaetoceros lorenzianus Grunow [2017]
Chaetoceros messanensis Castracane [2017]
Chaetoceros rostratus Ralfs in Lauder
Chaetoceros teres Cleve [2017]
Chaetoceros throndsenii (Marino, Montresor & Zingone) [2017]
Unidentified *Chaetoceros* spp.
Cerataulina pelagica (Cleve) Hendey
Cyclotella sp. [2017]
Dactyliosolen mediterraneus (H.Peragallo) H.Peragallo [2017]
Detonula pumila (Castracane) Gran [2017]
Ditylum brightwellii (T.West) Grunow
Eucampia groenlandica Cleve [2017]
Eucampia zodiacus Ehrenberg [2017]
Hemiaulus hauckii Grunow ex Van Heurck
Hemiaulus chinensis Greville
Lauderia annulata Cleve [2017]
Leptocylindrus danicus Cleve [2017]
Leptocylindrus minimus Gran [2017]
Skeletonema marinoi Sarno & Zingone
Thalassiosira gravida Cleve [2017]
Thalassiosira spp.
Unidentified centric diatoms
Unidentified pennate diatoms

Dinophyceae

Alexandrium catenella (Whedon & Kofoid) Balech [2016]
Alexandrium sp. [2016]
Amphidinium sp.
Azadinium caudatum (Halldal) Nézan & Chomérat [2017]
Balechina coerulea (Dogiel) F.J.R.Taylor [2017]
Cochlodinium spp.
Corythodinium constrictum (Stein) F.J.R.Taylor [2016]
Corythodinium diploconus (Stein) F.J.R.Taylor
Corythodinium tesselatum (Stein) Loeblich Jr. & Loeblich III [2016]
*Dicroerisma psilonereiella F.J.R.Taylor & S.A.Cattell
Dinophysis acuminata Claparède & Lachmann
Dinophysis caudata Seville-Kent
Dinophysis hastata Stein [2016]
Dinophysis sphaerica Stein
Dinophysis tripos Gourret [2017]

Table 1 (*continued*)

Bacillariophyta

Dinophysis sp.
Diplopsalis - complex
Gonyaulax birostris Stein [2016]
Gonyaulax digitalis (Pouchet) Kofoid [2016]
Gonyaulax fragilis (Schütt) Kofoid [2017]
Gonyaulax hyalina Ostenfeld & Schmidt [2017]
Gonyaulax milneri (G.Murray & Whitting) Kofoid [2016]
Gonyaulax polygramma Stein
Gonyaulax spinifera (Claparède & Lachmann) Diesing
Gonyaulax sp.
Gymnodinium spp.
Gyrodinium biconicum Kofoid & Swezy [2017]
Gyrodinium fusiforme Kofoid & Swezy
Gyrodinium spp.
Heterodinium globosum Kofoid
Histioneis joergensenii J.Schiller
Histioneis longicollis Kofoid
Histioneis sp. [2016]
Karenia papilionacea A.J.Haywood & K.A.Steidinger
Kofoidinium velleloides Pavillard [2016]
Lingulodinium polyedra (Stein) Dodge
Mesoporos perforatus (Gran) Lillick
Micracanthodinium setiferum (Lohmann) Deflandre [2016]
Noctiluca scintilans (Macartney) Kofoid & Swezy
Oxytoxum caudatum Schiller
Oxytoxum longiceps Schiller [2016]
Oxytoxum reticulatum (Stein) Schütt
Oxytoxum sceptrum (Stein) Schroder [2017]
Oxytoxum scolopax Stein
Oxytoxum sphaeroideum Stein
Oxytoxum turbo Kofoid
Oxytoxum variabile J. Schiller
Phalacroma mitra F.Schütt [2017]
Phalacroma ovum Schütt [2016]
Phalacroma oxytoxoides (Kofoid) F.Gomez, P.Lopez-Garcia & D.Moreira [2017]
Phalacroma rotundatum (Claparede et Lachmann) Kofoid & Michener
Podolampas bipes Stein
Podolampas palmipes Stein
Podolampas spinifera Okamura
*Pomatodinium impatiens J.Cachon & Cachon-Enjumet [2016]
Pronoctiluca pelagica Fabre-Domergue
Pronoctiluca rostrata F.J.R.Taylor [2016]
Pronoctiluca spinifera (Lohmann) Schiller
Prorocentrum cordatum (Ostenfeld) J.D.Dodge
Prorocentrum dactylus (Stein) Dodge [2016]
Prorocentrum micans Ehrenberg
Prorocentrum rostratum Stein [2017]
Prorocentrum scutellum Schröder
Prorocentrum triestinum J. Schiller
Protoceratium reticulatum (Claparède & Lachmann) Bütschli
Protoperidinium bipes (Paulsen) Balech [2016]
Protoperidinium brochii (Kofoid & Swezy) Balech
Protoperidinium cf. *pacificum* [2017]
Protoperidinium conicum (Gran) Balech [2017]
Protoperidinium crassipes (Kofoid) Balech
Protoperidinium cysts
Protoperidinium diabolus (Cleve) Balech [2017]
Protoperidinium divergens (Ehrenberg) Balech [2016]
Protoperidinium globulus (F.Stein) Balech
Protoperidinium oceanicum (Vanhöffen) Balech
Protoperidinium ovum (Schiller) Balech
Protoperidinium pallidum (Ostenfeld) Balech [2016]
Protoperidinium pellucidum Bergh
Protoperidinium pyriforme (Paulsen) Balech [2017]
Protoperidinium quarnerense (B.Schröder) Balech [2016]
Protoperidinium sphaericum (Murray & Whitting) Balech
Protoperidinium steinii (Jørgensen) Balech
Protoperidinium tuba (Schiller) Balech
Protoperidinium sp.
Scrippsiella spp.
Sourniaea diacantha (Meunier) H.Gu., K.N.Mertens, Zhun Li & H.H.Shin
Torodinium robustum Kofoid & Swezy
Triadinium polyedricum (Pouchet) J.D.Dodge
Tripos arietinus (Cleve) F.Gómez
Tripos azoricus (Cleve) F.Gómez
Tripos candelabrum (Ehrenberg) F.Gómez

Table 1 (*continued*)

Bacillariophyta
Tripos carriensis (Gourret) F.Gómez
Tripos furca (Ehrenberg) F.Gómez
Tripos fusus (Ehrenberg) F.Gómez
Tripos hexacanthus (Gourret) F.Gómez [2017]
Tripos horridus (Cleve) F.Gómez [2017]
Tripos kofoidii (Jörgenen) F.Gómez
Tripos longirostrus (Gourret) F.Gómez [2016]
Tripos macroceros (Ehrenberg) F.Gómez [2016]
Tripos massiliensis (Gourret) F.Gómez [2016]
Tripos muelleri Bory
Tripos pentagonus (Gourret) F.Gómez [2016]
Tripos pulchellus (Schröder) F.Gómez [2017]
Tripos setaceus (Jørgesen) F.Gómez [2017]
Tripos teres (Kofoid) F.Gómez
Tripos sp.
Noctilucophyceae
Scaphodinium mirabile Margalef
Spatulodinium pseudonoctiluca (Pouchet) J.Cachon & M.Cachon [2016]
Other unidentified dinoflagellates
Dinoflagellates cyst
Group of undetermined Nanoflagellates

Year in parentheses means that the taxon was found in the winter-spring period of the particular year only. Two taxa indicated by asterisk (*) before the scientific name was found for the first time for the Adriatic Sea.

winter-spring periods. Diatoms contributed to the phytoplankton abundance from 0.1 to 3% in 2016, and from 1 to 41% in 2017, respectively. With the exception of coccolithophorids (1–3%), the percentage contribution of other groups (dinoflagellates, silicoflagellates and chlorophytes) to total phytoplankton abundance was less than 1% throughout both winters-spring periods.

Among diatoms, unidentified pennate taxa (14–44.4%), *Bacillaria paxillifera* (31.3–31.9%) and *Nitzschia* spp. (5.8–17.6%) contributed most to diatom abundance in 2016 (Supplementary material S-4). In 2017, these were *Thalassionema nitzschioides* (12.5–51.3%) and unidentified pennate taxa (3.5–43.1%). Diatoms had the highest contribution to the phytoplankton abundance (21.1–41.0%) from 3th to 20th March 2017, with values from 6.1×10^2 to 5×10^4 cells L^{-1} and 2×10^2 to 1.9×10^5 cells L^{-1} on 3rd and 20th March, respectively (Supplementary material S-1). During the peak (20th March) diatoms were mostly composed of *Pseudo-nitzschia* spp. (19.8%), *Chaetoceros* spp. (13.4%), *Ch. lorenzianus* (12.0%), *Ch. affinis* (11.1%) and *Asterionellopsis glacialis* (9.6%). The majority of the diatom population occurred in the surface layer (0–50 m). Finally, four days later (24th March), diatom contribution markedly decreased (1%), while coccolithophorids contribution (2–3%) slightly increased.

No strong seasonal variation in coccolithophorid abundances was observed (Fig. 5). The highest values were in the layer 0–50 m in February 2016, and at 20 m depth in May 2017. *Syracosphaera pulchra* and *Calyptrosphaera oblonga* were the most abundant coccolithophorids, with their maximum of 2.0×10^3 cells L^{-1} and 1.7×10^3 cells L^{-1}, respectively (Supplementary material S-1, S-3).

Among dinoflagellates, *Tripos furca* was the most abundant (1.0×10^3 cells L^{-1}, at 150 m depth on 24th March 2017). In both study periods, a group of unidentified thechate forms (18.5–50.2%) and *Oxytoxum variabile* (6.7–27.4%) contributed most to the dinoflagellate abundance (Supplementary material S-3).

Silicoflagellates were composed only of *Dictyocha fibula* and *Octactis octonaria*, and both had low abundances and frequency of occurrences (Supplementary material S-1, S-4).

Among chlorophytes (only *H. viridis*), no regular pattern of species development was observed either over the study period or among the sampling depths (Fig. 5, Supplementary material S-4).

3.5. In-situ and satellite chlorophyll-a distribution

In general, chlorophyll-*a* concentrations (Chl-*a*) were higher in 2017 than in 2016 (Fig. 6). Chl-*a* maxima, derived either from the bottle samples (1.65 mg m^{-3} at 10 m depth) or CTD profiles (1.7–1.85 mg m^{-3}, in the layer between 12 and 42 m depth) were recorded on 20th March as evidence of diatom bloom peak (see also Fig. 5).

Satellite surface Chl-*a* maps (8-days average composite images) for the southern Adriatic showed that during two winter-spring periods the highest peak occurred in the second half of March 2017 (Supplementary material S-5, S-6).

3.6. Phytoplankton taxa and their relation to environmental variables (CCA)

In 2016, eigenvalues from the Canonical Correspondence Analysis (CCA) analysis for the first four axes were 0.415, 0.181, 0.095 and 0.085 (Fig. 7). The species–environmental correlation for the first and second axes was 0.923 and 0.847, respectively. The first two axes explain 58.2% of variance of species–environment relationship. Potential temperature (F = 5.99, P = 0.036), Chl-*a* (F = 2.99, P = 0.028), and NO$_2$ (F = 1.74, P = 0.048) were important factors influencing selected taxa of the phytoplankton community. Other variables were not significant. For example, *Coccolithus pelagicus*, *Calciosolenia brasiliensis*, *Syracosphaera histrica*, *Helicosphaera carteri*, etc. were associated with higher NO$_2$ values. *C. oblonga*, *Rhabdosphaera tignifer*, *S. pulchra* and *H. viridis* were associated with higher temperatures..

In 2017, eigenvalues from the CCA analysis for the first four axes were 0.466, 0.284, 0.156 and 0.090 (Fig. 7). The species–environmental correlation for the first and second axes was 0.915 and 0.783, respectively. The first two axes explain 66.9% of variance of species–environment relationship. Potential temperature (F = 12.03, P = 0.006) and Chl-*a* (F = 9.78, P = 0.018) were the most important related factors for selected taxa followed by TIN (including both NO$_3$ and NO$_2$), O$_2$/O$_2$' and potential density. Salinity was of less importance, while NH$_4$, SiO$_4$ and PO$_4$ were not significant. *T. nitzschioides* and *Hemiaulus hauckii* were associated with temperature, while the majority of selected taxa, grouped in the upper right quadrant, were closely related to NO$_3$. On the opposite side, the bloom-forming taxa, i.e. *Pseudo-nitzschia* spp., unidentified *Chaetoceros* spp., *Bacteriastrum delicatulum*, *Guinardia striata* and *Cerataulina pelagica* were not significantly associated by any of the considered variables.
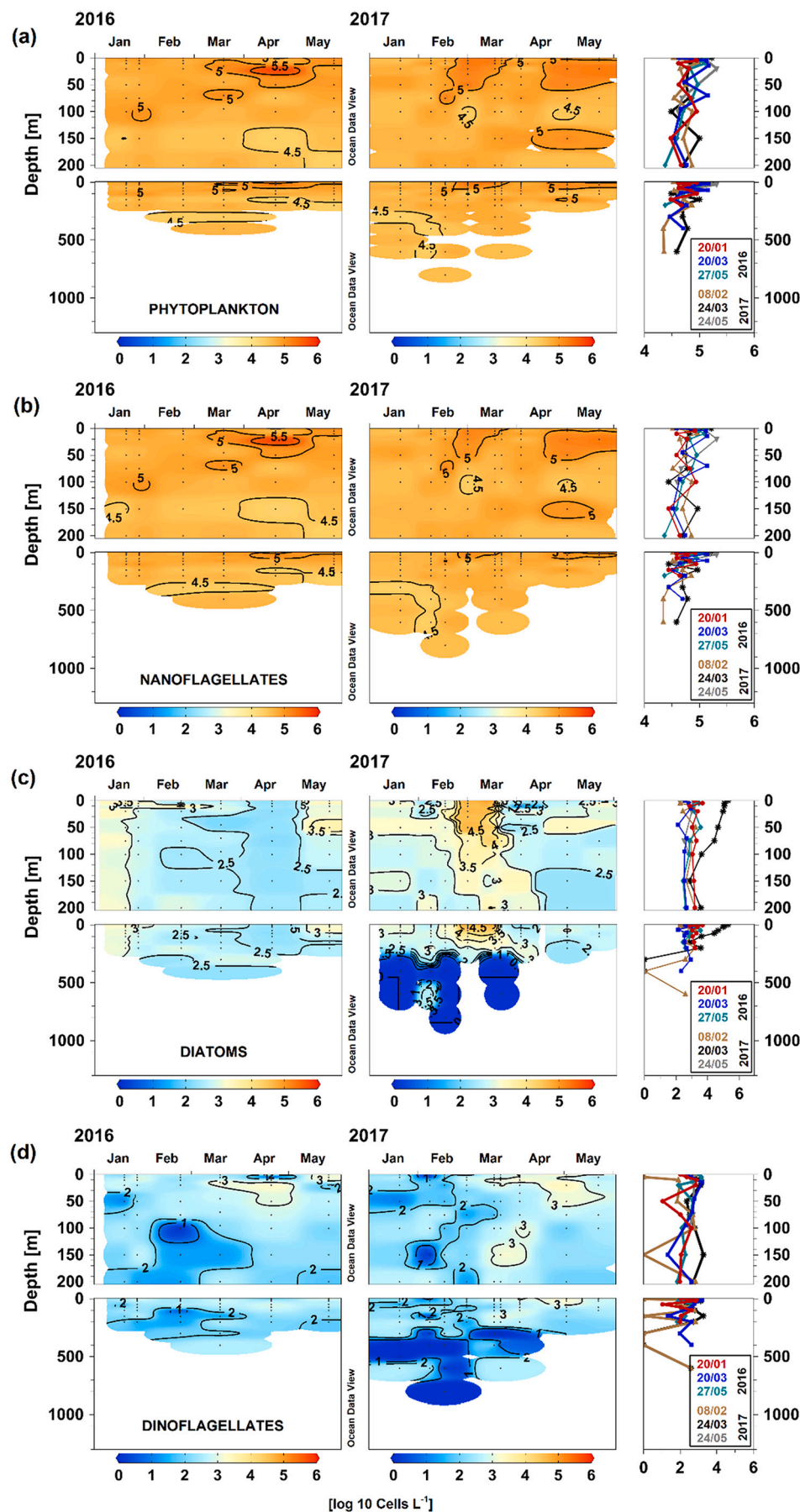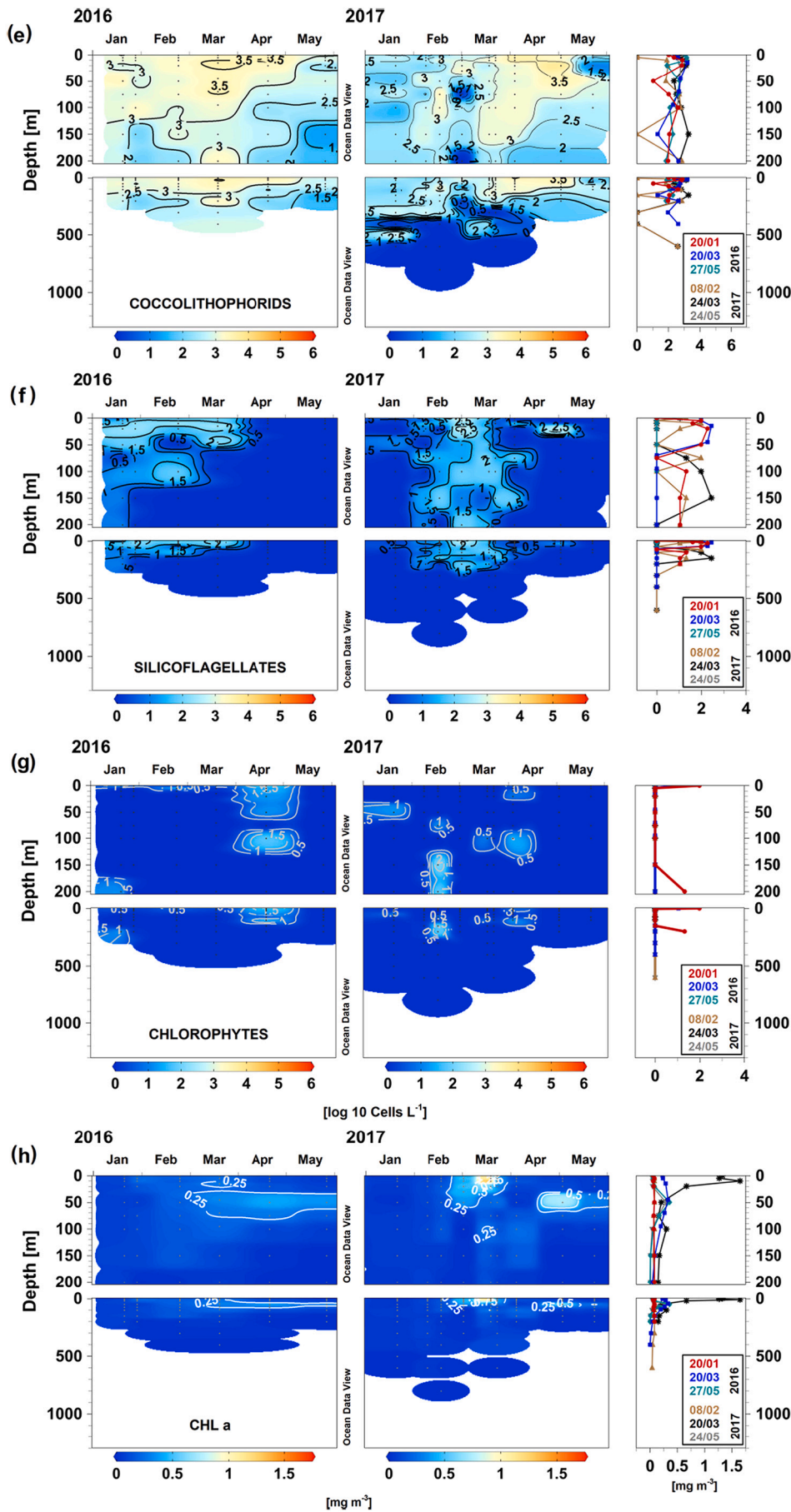
Fig. 5. Station P-1200 in the open southern Adriatic Sea: time evolution (on the left-hand side) and selected vertical profiles (on the right-hand side) of the cell abundance (log 10 cells L^{-1}), for total phytoplankton (a), nanoflagellates (b), diatoms (c), dinoflagellates (d), coccolithophorids (e), silicoflagellates (f) and chlorophytes (g), and Chl-*a* concentrations (mg m^{-3}) from the bottle samples (h) in two winter-spring periods (2016, 2017). Samples were taken at standard oceanographic depths (dots). The units for the plankton are indicated in (d) and (g). Topmost panels zoom into the upper 200 m.
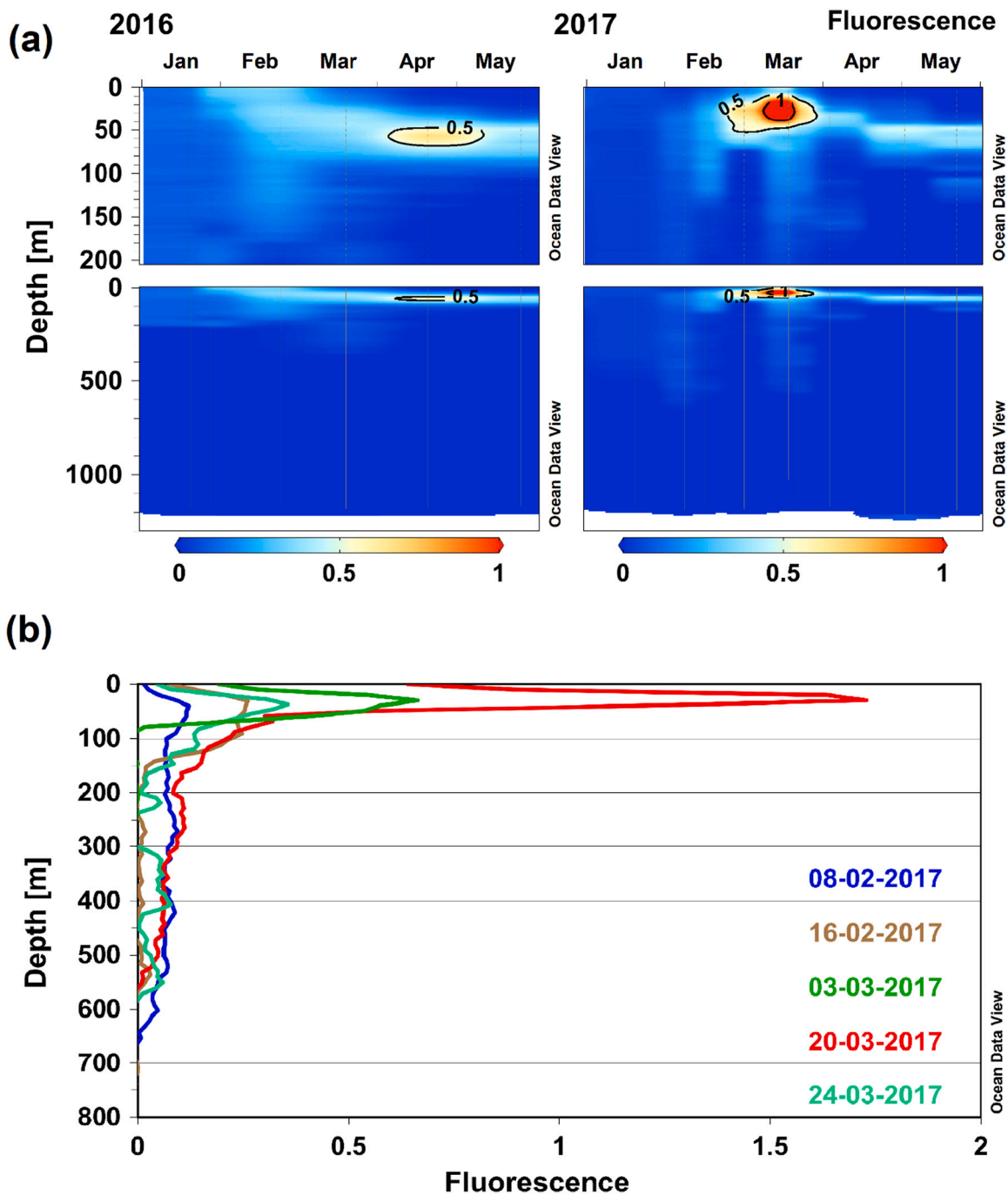
Fig. 6. Station P-1200 in the open southern Adriatic Sea: time evolution of fluorescence values (from CTD sensor, equivalent to chlorophyll-*a* concentration estimates, Chl-*a*, mg m^{-3}), during the winter-spring period in 2016 and 2017 (a), and the evolution of bloom event captured by Chl-*a* in the period from 8th February 2017 to 24th March 2017 (b).

4. Discussion

Different local atmospheric and marine conditions modified thermohaline properties in the SAP through vertical convection events and mixing that occurred in particular during winter-spring 2017. The vertical turnover homogenized the thermohaline properties in the water column and boosted the upward transport of nutrients. Consequently, as post-convection vertical stability conditions were restored, a phytoplankton (diatom) bloom in the euphotic zone was triggered in March 2017. On the contrary, in 2016, the effects of a limited vertical convection resulted in lower phytoplankton abundances. That might be a

direct consequence of a mild winter without strong Bura wind events.

The winter weather conditions are the main physical forcing mechanisms able to trigger vertical mixing processes as well as the formation of dense water in the southern Adriatic (Gačić et al., 2002; Bensi et al., 2013; Mihanović et al., 2018). The cooling and evaporation process acting at the sea surface during harsh meteorological events characterized by the outbreaks of cold, dry, and strong NE winds (Artegiani et al., 1997), indeed, cause water density increase at the sea surface, and the consequent convective movements that can homogenize the water column sometimes even down to 800–900 m depth (Bensi et al., 2013; and others). On the contrary, the persistence of southerly winds in the area,
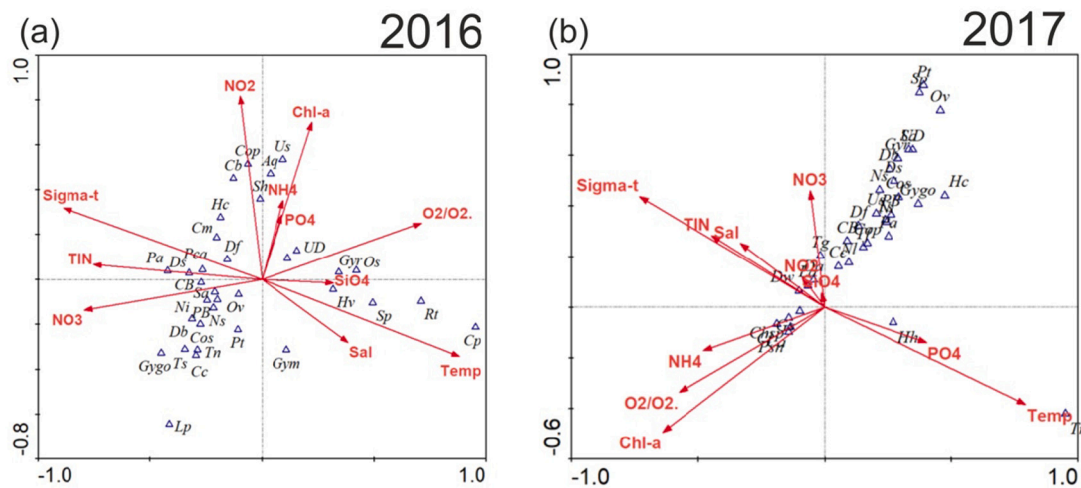
Fig. 7. CCA biplot showing 34 microphytoplankton taxa (triangle) found in more than 11% samples ($n = 47$) and vectors of the 11 environmental variables (arrows) in the winter-spring period in 2016 (a). A dataset of 37 microphytoplankton taxa found in more than 15% of the total number of samples ($n = 91$) was selected for analyses in the winter-spring period of 2017 (b). Abbreviations of taxa: Aq-*Acanthoica quattrospina*, As-*Asterionellopsis glacialis*, Bd-*Bacteriastrum delicatulum*, Cb-*Calciosolenia brasiliensis*, Cm-*Calciosolenia murrayi*, Cp-*Calyptrosphaera oblonga*, Ce-*Cerataulina pelagica*, Ca-*Chaetoceros affinis*, Cl-*Chaetoceros lorenzianus*, Cop-*Coccolithus pelagicus*, Cos-*Coscinodiscus* spp., Cc-*Cylindrotheca closterium*, Da-*Dactyliosolen fragilissimus*, Df-*Dictyocha fibula*, Db-*Diploneis bombus*, Ds-*Diploneis* spp., Dw-*Ditylum brightwellii*, Gs-*Guinardia striata*, Gym-*Gymnodinium* spp., Gyr-*Gyrodinium* spp., Gygo-*Gyrosigma* spp., Hv-*Halosphaera viridis*, Hc-*Helicosphaera carteri*, Hh-*Hemiaulus hauckii*, La-*Lauderia annulata*, Lp-*Lioloma pacificum*, Ns-*Navicula* spp., Nl-*Nitzschia longissima*, Ni-*Nitzschia* spp., Os-*Oxytoxum sphaeroideum*, Ov-*Oxytoxum variabile*, Pa-*Pleurosigma angulatum*, Pt-*Protoperidinium tuba*, Psn-*Pseudo-nitzschia* spp., Pca-*Pseudosolenia calcar-avis*, Rt-*Rhabdosphaera tignifer*, Sa-*Scyphosphaera apsteinii*, Sh-*Syracosphaera histrica*, Sp-*Syracosphaera pulchra*, Tf-*Thalassionema frauenfeldii*, Tn-*Thalassionema nitzschioides*, Tg-*Thalassiosira gravida*, Ts-*Thalassiosira* spp., Us-*Umbilicosphaera sibogae*, CB-unidentified centric diatoms, Chsp-unidentified *Chaetoceros* taxa, UD-unidentified dinoflagellates, PB-unidentified pennate diatoms.

on the one side prevents buoyancy loss and hence vertical convection, and on the other side favours the inflow of relatively warm water from the Ionian Sea.

The nutrient-rich reservoir during both winter-spring periods was located at high depths (> 400 m), but vertical convection and mixing is able to bring nutrients into the upper layer. At the beginning of March 2017, the diatom bloom started, reaching its maximum around two weeks later, as clearly shown by in-situ and satellite Chl-*a* data. It occurred during the greatest SiO_4, PO_4 and NH_4 availability. Similar abundances of diatoms in the SAP have been reported in previous studies (e.g., Cerino et al., 2012; Ljubimir et al., 2017; Batistić et al., 2019) in winter (February) and spring (March or April).

In general, the bloom-type diatom community (*Chaetoceros, Pseudo-nitzschia, Nitzschia,* etc.) suggests that a high nutrient environment supported the growth of species typical for the summer bloom of the southern Adriatic coastal waters, i.e. in areas of higher trophic levels and influenced by anthropogenic nutrient loads (cf., Jasprica and Carić, 2001; Jasprica et al., 2001). These species are generally the main contributors to high Chl-*a* in cases of intense physical dynamics, i.e., during winter convection, and within gyres, eddies and fronts (Siokou-Frangou et al., 2010; Batistić et al., 2019; Decembrini et al., 2020). Some species (e.g., *Skeletonema*) are well known to bloom regularly in nutrient-rich surface waters of the northern Adriatic Sea during February-March (Totti et al., 2005; Bernardi Aubry et al., 2012). Hence, in our case, they may originate from the northern Adriatic source area, and reach the deep SAP either by southward currents along the western Adriatic coast and/or by crosswise flow within the cyclonic gyre and mesoscale eddies from the eastern or western Adriatic coast (Borzelli et al., 1999; Bernardi Aubry et al., 2018). Furthermore, high phytoplankton abundances in deep layer from January to March 2016 associated with strong downward flow, can also be, at least partly, linked to the lower salinity and possible intrusion of coastal waters into the offshore area (Njire et al., 2019).

Rapid decrease of NO_3 during the Chl-*a* peak and diatom bloom may result from the assimilation by diatoms who prefer NO_3 as their N-source (Domingues et al., 2011). Our CCA results revealed that abundances of

some bloom-forming diatoms were also influenced by NO_3. Additionally, *Skeletonema marinoi* and *Chaetoceros* species that were dominant at the time, are both known to process nutrients rapidly into new biomass (Collos, 1986; Orefice et al., 2019). Furthermore, an increase of NH_4 in April 2017 can be attributed to phytoplankton cell degradation that started in the post-bloom period. Although the role of zooplankton was unfortunately not addressed in this study, we can hypothesize its contribution in controlling diatom growth and in excretion of NH_4 (Alcaraz et al., 1994). Increased NH_4 and seawater temperature in May 2016 and April 2017 favoured the dinoflagellates growth in a stratified water column, in accordance with studies reported by Dagenais-Bellefeuille and Morse (2013).

As expected, phytoplankton was largely composed by nanoflagellates and mainly represented by small forms of uncertain taxonomic identification, as reported for the southern Adriatic Sea (Socal et al., 1999; Cerino et al., 2012; Ljubimir et al., 2017; Decembrini et al., 2021). The exclusively dominance of nanoflagellates in phytoplankton spring bloom (April 2016) showed their particular importance during period of stratification and lower nutrient availability (Marañón, 2015, and references therein).

In our study, higher abundances of coccolithophorids and their contribution to total phytoplankton from late March to May may be at least partly related to higher temperature and NO_2 (revealed by CCA results), whereas the latter may be related to excretion by algal cells (Al-Qutob et al., 2002). Larger abundances of coccolithophorids in the surface layer (0–50 m depth) may be influenced by saltier waters inflowing from the Ionian Sea (Fonda Umani, 1996; Malinverno et al., 2003). Indeed our data show that, from March 2017 on, the surface layer was saltier than before.

The difficulties of identification and enumeration of some phytoplankton taxa due to limitations in light microscopy (LM) observations need to be stressed. A reliable identification of small nanoflagellates requires culture studies and analysis with scanning electron microscope (SEM). Bloom-forming diatom taxa could also not be identified to species level. In particular, *Nitzschia* spp. and other single-celled pennate diatoms need further especially careful LM and SEM analyses due to

their high contribution to the overall phytoplankton community in SAP (Batistić et al., 2012; Mucko et al., 2020).

According to our best knowledge, dinoflagellates *Dicroerisma psilonereiella* and *Pomatodinium impatiens* have not been recorded for the Adriatic Sea, yet. However, both species have already been found in Mediterranean Sea (Gómez and Furuya, 2007; Gómez, 2011), and their presence has gone unnoticed due to their small size, deep water distribution and misidentification with other gymnodinioid and nocticuloid cells, respectively.

5. Conclusion

This article provides a more detailed contribution to the current knowledge about the distribution of phytoplankton and their response to convective mixing, especially regarding the timing of the phytoplankton bloom development. We documented the frequency and magnitude of winter-spring convective events and bloom formations in SA during 2016 and 2017. The high abundances and biomass of phytoplankton in the SAP observed in March 2017 are the result of convection-driven nutrient enrichment in the upper layer, followed by a period of water column stability that promotes phytoplankton development. Deep water convection in winter is one of the major processes driving primary productivity in open waters, such as in the Southern Adriatic Sea (eastern Mediterranean Sea). This process is highly variable in time, depending on the specific oceanographic and meteorological conditions (circulation, stratification, sea-atmosphere interactions) of each specific winter. Phytoplankton community can be a good indicator of occurrence of such convective events. Nutrient availability and phytoplankton standing stocks in the Southern Adriatic Sea have shown a strong heterogeneity between the two years. However, long term studies of the phytoplankton community, especially during winter, are needed to have a better comprehension of the mechanisms that govern planktonic production and community variety.

Appendix A. Supplementary data

Supplementary data to this article can be found online at https://doi.org/10.1016/j.jmarsys.2021.103665.

References

Alcaraz, M., Saiz, E., Estrada, M., 1994. Excretion of ammonia by zooplankton and its potential contribution to nitrogen requirements for primary production in the Catalan Sea (NW Mediterranean). Mar. Biol. 119, 69–76. https://doi.org/10.1007/BF00350108.

Al-Qutob, M., Häse, C., Tilzer, M., Lazar, B., 2002. Phytoplankton drives nitrite dynamics in the Gulf of Aqaba, Red Sea. Mar. Ecol. Prog. Ser. 239, 233–239. Retrieved December 24, 2020 from. http://www.jstor.org/stable/24866062>.

Artegiani, A., Bregant, D., Paschini, E., Pinardi, N., Raicich, F., Russo, A., 1997. The Adriatic Sea general circulation. Part I: air-sea interactions and water mass structure. J. Phys. Oceanogr. 27, 1492–1514. doi.org/10.1175/1520-0485.

Babić, I., Petrić, I., Bosak, S., Mihanović, H., Dupčić Radić, I., Ljubešić, Z., 2017. Distribution and diversity of marine picocyanobacteria community: targeting of *Prochlorococcus* ecotypes in winter conditions (southern Adriatic Sea). Mar. Genomics 36, 3–11. https://doi.org/10.1016/j.margen.2017.05.014.

Batistić, M., Jasprica, N., Carić, M., Čalić, M., Kovačević, V., Garić, R., Njire, J., Mikuš, J., Bobanović-Čolić, S., 2012. Biological evidence of a winter convection event in the south Adriatic: a phytoplankton maximum in the aphotic zone. Cont. Shelf Res. 44, 57–71.

Batistić, M., Garić, R., Molinero, J.C., 2014. Interannual variations in Adriatic Sea zooplankton mirror shifts in circulation regimes in the Ionian Sea. Clim. Res. 61, 231–240. https://doi.org/10.3354/cr01248.

Batistić, M., Viličić, D., Kovačević, V., Jasprica, N., Garić, R., Lavigne, H., Carić, M., 2019. Occurrence of winter phytoplankton bloom in the open southern Adriatic: relationship with hydroclimatic events in the eastern Mediterranean. Cont. Shelf Res. 174, 12–25.

Bensi, M., Cardin, V., Rubino, A., Notarstefano, G., Poulain, P.M., 2013. Effects of winter convection on the deep layer of the southern Adriatic Sea in 2012. J. Geophys. Res. C Oceans 118, 6064–6075. https://doi.org/10.1002/2013JC009432.

Bernardi Aubry, F., Cossarini, G., Acri, F., Bastianini, M., Bianchi, F., Camatti, E., De Lazzari, A., Pugnetti, A., Solidoro, C., Socal, G., 2012. Plankton communities in the northern Adriatic Sea: patterns and changes over the last 30 years. Estuar. Coast. Shelf Sci. 115, 125–137. https://doi.org/10.1016/j.ecss.2012.03.011.

Bernardi Aubry, F., Falcieri, F.M., Chiggiato, J., Boldrin, A., Luna, G.M., Finotto, S., Camatti, E., Acri, F., Sclavo, M., Carniel, S., Bongiorni, L., 2018. Massive shelf dense water flow influences plankton community structure and particle transport over long distance. Sci. Rep. 8, 4554. https://doi.org/10.1038/s41598-018-22569-2.

Boldrin, A., Miserocchi, S., Rabitti, S., Turchetto, M.M., Balboni, V., Socal, G., 2002. Particulate matter in the southern Adriatic and Ionian Sea: characterization and downward fluxes. J. Mar. Syst. 33-34, 389–410.

Borzelli, G., Manzella, G., Marullo, S., Santoleri, R., 1999. Observations of coastal filaments in the Adriatic Sea. J. Mar. Syst. 20, 187–203.

Cerino, F., Bernardi Aubry, F., Coppola, J., La Ferla, R., Maimone, G., Socal, G., Totti, C., 2012. Spatial and temporal variability of pico-, nano- and microphytoplankton in the offshore waters of the southern Adriatic Sea (Mediterranean Sea). Cont. Shelf Res. 44, 94–105. https://doi.org/10.1016/j.csr.2011.06.006.

Civitarese, G., Gačić, M., Lipizer, M., Borzelli, G.L.E., 2010. On the impact of the bimodal oscillating system (BiOS) on the biogeochemistry and biology of the Adriatic and Ionian seas (eastern Mediterranean). Biogeosciences 7, 3987–3997.

Clarke, K.R., Gorley, R.N., 2006. PRIMERv6: User Manual/Tutorial (Plymouth Routines in Multivariate Ecological Research). PRIMER-E, Plymouth.

Collos, Y., 1986. Time-lag algal growth dynamics: biological constraints on primary production in aquatic environments. Mar. Ecol. Prog. Ser. 33, 193–206.

Dagenais-Bellefeuille, S., Morse, D., 2013. Putting the N in dinoflagellates. Front. Microbiol. 4, 369. https://doi.org/10.3389/fmicb.2013.00369.

Decembrini, F., Caroppo, C., Bergamasco, A., 2020. Influence of lateral advection on phytoplankton size-structure and composition in a Mediterranean coastal area. Cont. Shelf Res. 209, 104216. https://doi.org/10.1016/j.csr.2020.104216.

Decembrini, F., Caroppo, C., Caruso, G., Bergamasco, A., 2021. Linking microbial functioning and trophic pathways to ecological status in a coastal Mediterranean ecosystem. Water 13 (9), 1325. https://doi.org/10.3390/w13091325.

Domingues, R.B., Barbosa, A.B., Sommer, U., Galvão, H.M., 2011. Ammonium, nitrate and phytoplankton interactions in a freshwater tidal estuarine zone: potential effects of cultural eutrophication. Aquat. Sci. 73, 331–343.

Fonda Umani, S., 1996. Pelagic production and biomass in the Adriatic Sea. Sci. Mar. 60 (2), 65–77.

Gačić, M., Civitarese, G., 2012. Introductory notes on the south Adriatic oceanography. Cont. Shelf Res. 44, 2–4.

Gačić, M., Civitarese, G., Ursella, L., 1999. Spatial and seasonal variability of water and biogeochemical fluxes in the Adriatic Sea. In: Malanotte-Rissoli, P., Eremeev, V.N.

(Eds.), The Eastern Mediterranean as a Laboratory for Basin for the Assessment of Contracting Ecosystems. Kluwer Academic Publishing, Dordrecht, The Netherlands, pp. 335–357.

Gačić, M., Civitarese, G., Miserocchi, S., Cardin, V., Crise, A., Mauri, E., 2002. The open-ocean convection in the southern Adriatic: a controlling mechanism of the spring phytoplankton bloom. Cont. Shelf Res. 23 (14), 1897–1908. https://doi.org/10.1016/S0278-4343(02)00050-X.

Gačić, M., Borzelli, G.L.E., Civitarese, G., Cardin, V., Yari, S., 2010. Can internal processes sustain reversals of the ocean upper circulation? The Ionian Sea example. Geophys. Res. Lett. 37 (9), L09608 https://doi.org/10.1029/2010GL043216.

Gómez, F., 2011. First records of the dinoflagellate genus *Dicroerisma* (Actiniscales, Dinophyceae) in the Mediterranean Sea. Acta Adriat. 52, 149–154.

Gómez, F., Furuya, K., 2007. Kofoidinium, Spatulodinium and other kofoidiniaceans (Noctilucales, Dinophyceae) in the Pacific Ocean. Eur. J. Protistol. 43, 115–124.

Grbec, B., Dulčić, J., Morović, M., 2002. Long-term changes in landings of small pelagic fish in the eastern Adriatic – possible influence of climate oscillations over the northern hemisphere. Clim. Res. 20, 241–252.

Guiry, M.D., Guiry, G.M., 2020. AlgaeBase.World-wide electronic publication, National University of Ireland, Galway. Retrieved August 4, 2020 from. http://www.algaebase.org.

Holm-Hansen, O., Lorenzen, C.J., Holmes, R.W., Strickland, J.D.H., 1965. Fluorometric determination of chlorophyll. J. Conseil 30, 3–15.

Ivančić, I., Degobbis, D., 1984. An optimal manual procedure for ammonia analysis in natural waters by the indophenol blue method. Water Res. 18, 1143–1147.

Jasprica, N., Carić, M., 2001. Planktonic diatoms and their relation to environmental factors at three stations in the southern Adriatic, Mediterranean Sea. In: Jahn, R., Kociolek, J.P., Witkowski, A., Compère, P. (Eds.), Lange-Bertalot-Festschrift: Studies on Diatoms. Gantner, Ruggell, Berlin, pp. 513–536.

Jasprica, N., Carić, M., Viličić, D., 2001. Relationships of subsurface chlorophyll maximum to diatoms and other microphytoplankton in the southern Adriatic Sea. In: Economou-Ammilli, A. (Ed.), The Proceedings of the 16th International Diatom Symposium. Amvrosiou Press, Athens, Greece, pp. 365–379.

Legendre, L., Legendre, P., 1983. Numerical ecology. Elsevier, Amsterdam.

Ljubimir, S., Jasprica, N., Čalić, M., Hrustić, E., Dupčić Radić, I., Car, A., Batistić, M., 2017. Interannual (2009–2013) variability of winter-spring phytoplankton in South Adriatic Sea: effects of deep convection and lateral advection. Cont. Shelf Res. 143, 311–321.

Malinverno, E., Ziveri, P., Corselli, C., 2003. Coccolithophorid distribution in the Ionian Sea and its relationship to eastern Mediterranean circulation during late fall to early winter 1997. J. Geophys. Res. 108 (C9), 1–16. https://doi.org/10.1029/2002JC001346.

Manca, B.B., Budillo, G., Scarazzato, P., Ursella, L., 2003. Evolution of dynamics in the eastern Mediterranean affecting water mass structures and properties in the Ionian and Adriatic Sea. J. Geophys. Res. 108 (C9), 8102.

Marañón, E., 2015. Cell size as a key determinant of phytoplankton metabolism and community structure. Annu. Rev. Mar. Sci. 7, 241–264. https://doi.org/10.1146/annurev-marine-010814-015955.

Mihanović, H., Janeković, I., Vilibić, I., Kovačević, V., Bensi, M., 2018. Modelling interannual changes in dense water formation on the northern Adriatic shelf. Pure Appl. Geophys. 175, 4065–4081. https://doi.org/10.1007/s00024-018-1935-5.

Mucko, M., Bosak, S., Mann, D.G., Trobajo, R., Wetzel, C.E., Peharec Štefanić, P., Ljubešić, Z., 2020. A polyphasic approach to the study of the genus *Nitzschia* (Bacillariophyta): three new planktonic species from the Adriatic Sea. J. Phycol. https://doi.org/10.1111/jpy.13085.

Najdek, M., Paliaga, P., Šilović, T., Batistić, M., Garić, R., Supić, N., Ivančić, I., Ljubimir, S., Korlević, M., Jasprica, N., Hrustić, E., Dupčić-Radić, I., Blažina, M., Orlić, S., 2014. Picoplankton community structure before, during and after convection event in the offshore waters of the southern Adriatic Sea. Biogeosciences 11, 2645–2659. https://doi.org/10.5194/bg-11-2645-2014.

Njire, J., Batistić, M., Kovačević, V., Garić, R., Bensi, M., 2019. Tintinnid ciliate communities in pre- and post-winter conditions in the southern Adriatic Sea (NE Mediterranean). Water 11 (11), 2329. https://doi.org/10.3390/w11112329.

Orefice, I., Musella, M., Smerilli, A., Sansone, C., Chandrasekaran, R., Corato, F., Brunet, C., 2019. Role of nutrient concentrations and water movement on diatom's productivity in culture. Sci. Rep. 9, 1479. https://doi.org/10.1038/s41598-018-37611-6.

Poulain, P.M., Cushman-Roisin, B., 2001. Circulation. In: Cushman-Roisin, B., Gačić, M., Poulain, P.M., Artegiani, A. (Eds.), Physical Oceanography of the Adriatic Sea. Springer, Dordrecht, pp. 67–109. https://doi.org/10.1007/978-94-015-9819-4_3.

Robinson, A.R., Leslie, W.G., Theocharis, A., Lascaratos, A., 2001. Mediterranean Sea circulation. In: Steele, J.H., Thorpe, S.A., Turekian, K.K. (Eds.), Encyclopedia of Ocean Sciences. Elsevier, Amsterdam, The Netherlands, pp. 1689–1705.

Rubino, A., Hainbucher, D., 2007. A large abrupt change in the abyssal water masses of the eastern Mediterranean. Geophys. Res. Lett. 34, L23607 https://doi.org/10.1029/2007GL031737.

Santoleri, R., Banzon, V., Marullo, S., Napolitano, E., D'Ortenzio, F., Evans, R., 2003. Year-to-year variability of the phytoplankton bloom in the southern Adriatic Sea (1998–2000): sea-viewing wide field-of-view sensor observations and modelling study. J. Geophys. Res. 108, 8122. https://doi.org/10.1029/2002JC001636.

Schlitzer, R., 2020. Ocean Data View User's Guide Version 5.3.0, Ocean Data View. Retrieved November 27, 2020 from. https://odv.awi.de.

Šilović, T., Mihanović, H., Batistić, M., Dupčić Radić, I., Hrustić, E., Najdek, M., 2018. Picoplankton distribution influenced by thermohaline circulation in the southern Adriatic. Cont. Shelf Res. 155, 21–33. https://doi.org/10.1016/j.csr.2018.01.007.

Siokou-Frangou, I., Christaki, U., Mazzocchi, M.G., Montresor, M., Ribera d'Alcala, M., Vaque, D., Zingone, A., 2010. Plankton in the open Mediterranean Sea: a review. Biogeosciences 7, 1543–1586.

Socal, G., Boldrin, A., Bianchi, F., Civitarese, G., De Lazzari, A., Rabitti, S., Totti, C., Turchetto, M.M., 1999. Nutrients, particulate matter and phytoplankton variability in the photic layer of the Otranto Strait. J. Mar. Syst. 20, 381–398.

Strickland, J.D.H., Parsons, T.R., 1972. A Practical Handbook of Seawater Analysis. Fisheries Research Board of Canada, Ottawa, p. 310.

ter Braak, C.J.F., Šmilauer, P., 2002. CANOCO Reference Manual and CanoDraw for Windows User's Guide: Software for Canonical Community Ordination (version 4.5). Microcomputer Power, Ithaca, New York.

ter Braak, C.J.F., Verdonschot, P.F.M., 1995. Canonical correspondence analysis and related multivariate methods in aquatic ecology. Aquat. Sci. 57, 255–289.

Totti, C., Cangini, M., Ferrari, C., Kraus, R., Pompei, M., Pugnetti, A., Romagnoli, T., Vanucci, S., Socal, G., 2005. Phytoplankton size-distribution and community structure in relation to mucilage occurrence in the northern Adriatic Sea. Sci. Total Environ. 353, 204–217.

Turchetto, M.M., Bianchi, F., Boldrin, A., Malagutti, A., Rabitti, S., Socal, G., Strada, L., 2000. Nutrients, phytoplankton and primary production processes in oligotrophic areas (southern Adriatic and northern Ionian Sea). In: Atti Associazione Italiana Oceanologia Limnologia, 13, pp. 269–278.

UNESCO, 1987. International Oceanographic Tables, vol. 4. UNESCO, Paris.

Ursella, L., Kovačević, V., Gačić, M., 2011. Footprints of mesoscale eddy passages in the strait of Otranto (Adriatic Sea). J. Geophys. Res. 116, C04005 https://doi.org/10.1029/2010JC006633.

Utermöhl, H., 1958. Zur Ver vollkommung der quantitativen phytoplankton-methodik. In: Mitteilung Internationale Vereinigung Fuer Theoretische unde Amgewandte Limnologie, 9, pp. 1–38.

Vilibić, I., Orlić, M., 2002. Adriatic water masses, their rates of formation and transport through the Otranto Strait. Deep Sea Res. Part I 49, 1321–1340.

Viličić, D., 1998. Phytoplankton taxonomy and distribution in the offshore southern Adriatic. Natura Croatica 7, 127–141.

Viličić, D., Vučak, Z., Škrivanić, A., Gržetić, Z., 1989. Phytoplankton blooms in the oligotrophic open south Adriatic waters. Mar. Chem. 28 (1–3), 89–107.

Viličić, D., Leder, N., Gržetić, Z., Jasprica, N., 1995. Microphytoplankton in the strait of Otranto (eastern Mediterranean). Mar. Biol. 123, 619–630.

Weiss, R.F., 1970. The solubility of nitrogen, oxygen and argon in water and seawater. Deep-Sea Res. Oceanogr. Abstr. 17 (4), 721–735.

Yari, S., Kovačaević, V., Cardin, V., Gačić, M., Bryden, H.L., 2012. Direct estimate of water, heat, and salt transport through the strait of Otranto. J. Geophys. Res. 117, C09009 https://doi.org/10.1029/2012JC007936.